Decadal Trends in Evaporation from Global Energy and Water Balances

YONGQIANG ZHANG,* RAY LEUNING,+ FRANCIS H. S. CHIEW,* ENLI WANG,* LU ZHANG,* CHANGMING LIU,# FUBAO SUN,@ MURRAY C. PEEL,& YANJUN SHEN,** AND MARTIN JUNG++

* *CSIRO Water for a Healthy Country National Research Flagship, CSIRO Land and Water, Canberra, Australian Capital Territory, Australia*
+ *CSIRO Marine and Atmospheric Research, Canberra, Australian Capital Territory, Australia*
# *Institute of Geographic Sciences and Natural Resources Research, The Chinese Academy of Sciences, Beijing, China*
@ *Research School of Biology, The Australian National University, Canberra, Australian Capital Territory, Australia*
& *Department of Infrastructure Engineering, The University of Melbourne, Melbourne, Victoria, Australia*
** *Key Laboratory of Agricultural Water Resources, Center for Agricultural Resources Research, The Chinese Academy of Sciences, Shijiazhuang, China*
++ *Max Planck Institute for Biogeochemistry, Jena, Germany*

(Manuscript received 8 February 2011, in final form 27 July 2011)

ABSTRACT

Satellite and gridded meteorological data can be used to estimate evaporation (E) from land surfaces using simple diagnostic models. Two satellite datasets indicate a positive trend (first time derivative) in global available energy from 1983 to 2006, suggesting that positive trends in evaporation may occur in ''wet'' regions where energy supply limits evaporation. However, decadal trends in evaporation estimated from water balances of 110 wet catchments ($\overline{E}_{wb}$) do not match trends in evaporation estimated using three alternative methods: 1) $\overline{E}_{MTE}$, a model-tree ensemble approach that uses statistical relationships between E measured across the global network of flux stations, meteorological drivers, and remotely sensed fraction of absorbed photosynthetically active radiation; 2) $\overline{E}_{Fu}$, a Budyko-style hydrometeorological model; and 3) $\overline{E}_{PML}$, the Penman–Monteith energy-balance equation coupled with a simple biophysical model for surface conductance. Key model inputs for the estimation of $\overline{E}_{Fu}$ and $\overline{E}_{PML}$ are remotely sensed radiation and gridded meteorological fields and it is concluded that these data are, as yet, not sufficiently accurate to explain trends in E for wet regions. This provides a significant challenge for satellite-based energy-balance methods. Trends in $\overline{E}_{wb}$ for 87 ''dry'' catchments are strongly correlated to trends in precipitation ($R^2 = 0.85$). These trends were best captured by $\overline{E}_{Fu}$, which explicitly includes precipitation and available energy as model inputs.

1. Introduction

The quantity of water available for runoff (Q) and changing the amount of moisture stored in catchments is the difference between precipitation (P) and evaporation (E). Runoff from river basins is substantial in humid regions where P exceeds E, but there is little or no runoff in arid regions where $E \approx P$. Between these extremes, runoff is often the small residual between P and E and subtle changes in either can strongly affect water yields. Global warming associated with rising atmospheric CO_2 concentrations is expected to substantially modify the global hydrological cycle (Huntington 2006; Milly et al. 2005) and thus change the balance between P, E, and Q by differing amounts in various regions across the globe. Evaporation from land surfaces is fundamentally determined by the availability of water and energy, and understanding the contributions of trends and changing patterns in water and energy supply to changing evaporation is an important issue for earth system science. Suggested reasons for variations in E and Q include changes in precipitation (Zhang et al. 2007), the impact of global brightening/dimming on available energy (Roderick and Farquhar 2002; Wild et al. 2008, 2005), the coupled changes in photosynthesis and surface conductance due to enhanced greenhouse gas concentrations (Gedney et al. 2006), decreases in soil moisture content (Jung et al. 2010), and changes in land use or land cover (Piao et al. 2007). To identify possible causes for changes in E, Jung et al. (2010) used the model-tree ensemble (MTE) algorithm of Jung

Corresponding author address: Yongqiang Zhang, CSIRO Land and Water, P.O. Box 1666, Canberra ACT 2601, Australia.
E-mail: yongqiang.zhang@csiro.au

DOI: 10.1175/JHM-D-11-012.1

© 2012 American Meteorological Society

et al. (2009) to calculate monthly evaporation rates (E_{MTE}) for the global land surface from 1982 to 2008. The MTE is a machine-learning algorithm trained using evaporation measurements from the global Flux Network (FLUXNET) database, gridded global meteorological data, and remotely sensed fraction of absorbed photosynthetically active radiation. According to this algorithm, global average E_{MTE} increased by 0.71 ± 0.1 mm yr^{-2} from 1982 to 1997, but with a slight decreasing trend in E_{MTE} in the following decade. An ensemble of outputs from nine independent models gave similar results, and Jung et al. (2010) attributed the reduction in E_{MTE} in the past decade to declining soil water availability (i.e., precipitation), particularly across Africa and Australia where microwave remote sensing–based soil moisture data showed negative trends. This paper complements the work of Jung et al. (2010) by comparing four different approaches to estimating global and regional trends in evaporation from 1983 to 2006: 1) using the water balances of large, unregulated catchments ($\overline{E}_{wb}$); 2) through the model-tree ensemble approach of Jung et al. (2010) (E_{MTE}); 3) application of a classical ''Budyko'' hydrometeorological model ($\overline{E}_{Fu}$) (Fu 1981); and 4) through an energy-balance model that utilizes gridded meteorological data and remotely sensed radiation and leaf area index data ($\overline{E}_{PML}$) (Leuning et al. 2008). The energy-balance approach is particularly useful for assessing whether trends in E can be explained by key biological and meteorological variables other than precipitation.

Section 2 provides a brief summary of methods used for the evaporation calculations, while section 3 documents the data sources used in the analysis. Results are presented in section 4, followed by the discussion in section 5 and conclusions in section 6.

2. Modeling and estimation approaches

We first clarify our notation before introducing the estimation approaches used. Variables E_{MTE}, E_{PML}, P, and Q represent monthly or annual values, while $\overline{E}_{MTE}$, $\overline{E}_{PML}$, $\overline{P}$, $\overline{E}_{wb}$, $\overline{E}_{Fu}$, and $\overline{Q}$ indicate 5- or 23-yr (1983–2006) averages. Trends in all of the variables are for 5-yr running averages or 3-yr block averages.

a. Catchment water balances

Annual evaporation rates were calculated from the water balances of unregulated catchments using

$$\overline{E}_{wb} = \overline{P} - \overline{Q}. \quad (1)$$

Over the long term, the change in water storage is assumed to be negligible in unregulated catchments, allowing this term to be neglected when estimating $\overline{E}_{wb}$ (Zhang et al. 2001). Use of Eq. (1) also assumes precipitation is the only source of water in the catchment and evaporation the only loss; that is, no water is gained or lost via interbasin transfers (a leaky catchment; Le Moine et al. 2007) or via deep groundwater.

b. ''Budyko-curve'' hydrometeorological model

In this paper we use the form of the Budyko model given by Fu (1981):

$$\frac{\overline{E}_{Fu}}{\overline{P}} = 1 + \frac{\overline{E}_p}{\overline{P}} - \left[1 + \left(\frac{\overline{E}_p}{\overline{P}}\right)^{\omega}\right]^{1/\omega}, \quad (2)$$

in which ω is a parameter and $\overline{E}_P$ is the mean annual potential evaporation calculated by summing daily potential evaporation:

$$\overline{E}_p = \alpha_{PT} \sum_{1}^{365} [\varepsilon(A_i/\lambda)/(\varepsilon + 1)], \quad (3)$$

and where $\alpha_{PT} = 1.26$ (Priestley and Taylor 1972). Here A_i is the available energy for each 24-h day, λ is the latent heat of evaporation, and $\varepsilon = s/\gamma$, in which γ is the psychrometric constant and $s = de^*/dT$—the slope of the curve relating saturation water vapor pressure to temperature. A single value, $\omega = 2.48$, was used in Eq. (2) for all catchments globally. Its value was calibrated using water balances of gauged, unregulated catchments, averaged over the period 1983–2006 (Zhang et al. 2010).

c. Penman–Monteith combination equation

To separate explicitly the contributions of vegetation and soil to total evaporation, Leuning et al. (2008) modified the classic Penman–Monteith (PM) combination equation (Monteith 1964) according to

$$\lambda E_{PML} = \frac{f\varepsilon A_s}{\varepsilon + 1} + \frac{\varepsilon A_c + (\rho c_p/\gamma) D_a G_a}{\varepsilon + 1 + G_a/G_c}, \quad (4)$$

where $A_s = \tau A_i$ and $A_c = (1 - \tau)A_i$ are the flux density of available energy absorbed each day by the soil and canopy, respectively; $\tau = \exp(-k_A L_{ai})$; L_{ai} is leaf area index; k_A is the extinction coefficient for net radiation; ρ the density of air; and c_p the specific heat of air at constant pressure.

Term 1 on the right is used to estimate evaporation from the soil by multiplying the equilibrium evaporation rate at the soil surface, $\varepsilon A_s/(1 + \varepsilon)$, by a coefficient f that varies from $f = 1$ when the soil surface is wet to $f = 0$ when it is dry. In this paper we follow Zhang et al. (2010) in calculating the temporal variation of f as a function of precipitation and equilibrium evaporation rates for one month before and after the current 1-month time step.

TABLE 1. Comparison of mean annual evaporation rates E for the global land surface, wet pixels (where the aridity index $A_I \leq 1.5$), and dry pixels (where $A_I > 1.5$) for the period 1983–2006. Volume of water evaporated annually is also shown. Here $\overline{E}_{MTE}$ is missing in Sahara and Greenland where $\overline{E}_{PML}$ values are not included for global aggregation.

	Mean evaporation rate mm yr^{-1}		Volume evaporated 10^3 km^3 yr^{-1}			
Area	$\overline{E}_{MTE}$	$\overline{E}_{PML}$	$\overline{V}_{MTE}$	$\overline{V}_{PML}$	Trenberth et al. (2007)	Oki and Kanae (2006)
Global	521.5	563.2	61.3	66.2	73	65.5
Wet	645.2	729.6	26.6	30.0		
Dry	454.9	473.6	34.8	36.2		

Term 2 describes evaporation from the plant canopy. It is a function of A_c; D_a, the water vapor pressure deficit of the air at a reference height above the canopy; and G_a, the aerodynamic conductance. In addition to these meteorological variables, calculation of canopy evaporation requires knowledge of the canopy conductance G_c. This biophysical variable was estimated using the following simple model (Isaac et al. 2004; Leuning et al. 2008):

$$G_c = \frac{g_{sx}}{k_Q} \ln\left[\frac{Q_h + Q_{50}}{Q_h \exp(-k_Q L_{ai}) + Q_{50}}\right]\left(\frac{1}{1 + D_a/D_{50}}\right), \quad (5)$$

where g_{sx} is the apparent maximum stomatal conductance of leaves at the top of the canopy, k_Q is the extinction coefficient for visible radiation, and Q_h is the average flux density of visible radiation at the top of the canopy. The parameters Q_{50} and D_{50} are the values of Q_h and D_a, respectively, at which stomatal conductance is half its maximum value. The canopy conductance G_c varies with Q_h and D_a on all time scales and with L_{ai} at seasonal time scales. Equation (5) contains no explicit dependence of G_c on soil moisture because we wish to apply Eqs. (4) and (5) using remotely sensed and gridded meteorological data only. While this is a deficiency in the model, G_c does depend indirectly on long-term variation in soil water availability through the landscape-scale adjustment of D_a and L_{ai}—the so-called ''ecological equilibrium'' concept.

Four of the five parameters in Eqs. (4) and (5) [called the Penman-Monteith-Leuning (PML) model] were assigned constant values ($k_Q = k_A = 0.6$, $Q_{50} = 30$ W m^{-2}, and $D_{50} = 0.7$ kPa; Leuning et al. 2008). Following Zhang et al. (2010), the magnitude of the fifth parameter g_{sx} was estimated separately for each 0.5° land surface pixel used in our analysis by adjusting g_{sx} to force agreement between the 23-yr averages of $\overline{E}_{PML}$ and $\overline{E}_{Fu}$ for that pixel. Note, this does not force the trends (first time derivative) in $\overline{E}_{PML}$ and $\overline{E}_{Fu}$ to be the same over the averaging period. An advantage of E_{PML} is that it can be evaluated at fine temporal resolution and it allows us to examine the relative importance of key variables other than A that control evaporation, namely D_a, G_a, L_{ai}, and f. The advantage of $\overline{E}_{Fu}$ is that it explicitly includes precipitation as an input variable, whereas $\overline{E}_{PML}$ only uses P in calculating the soil wetness variable f.

We used the above equations to estimate $\overline{E}_{Fu}$ and g_{sx} and, thence, monthly E_{PML} of land surfaces at a 0.5° resolution globally for the period 1983–2006. The results were used to assess whether trends in $\overline{E}_{wb}$ calculated

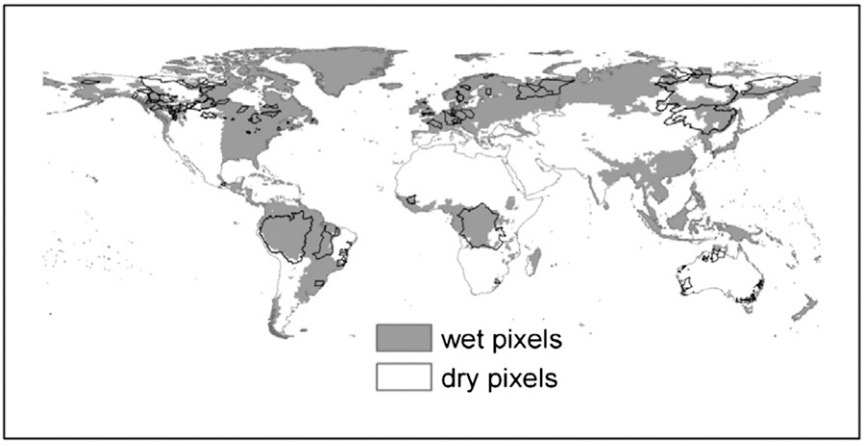

FIG. 1. Spatial pattern of wet pixels (aridity index; $A_I \leq 1.5$) and dry pixels ($A_I > 1.5$) across global land surface. Boundaries for the 197 unregulated catchments are shown in black.

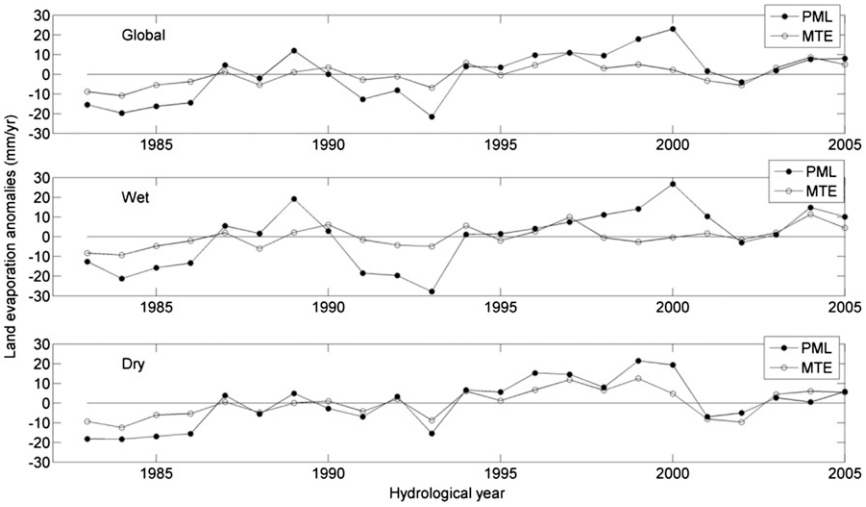

FIG. 2. Time series of annual evaporation E_{PML} and E_{MTE} for (top) the global land surface, (middle) wet catchments, and (bottom) dry catchments.

from catchment water balances are consistent with 1) trends in $\overline{E}_{Fu}$ due to variation in A and P; 2) with trends in $\overline{E}_{PML}$ resulting from those in A, D_a, G_a, L_{ai}, and f; or 3) with trends in $\overline{E}_{MTE}$ derived by Jung et al. (2010).

3. Data and methods

To calculate monthly E_{PML} we used monthly meteorological fields of daytime average air temperature and humidity to calculate D_a and G_a, while A_c, A_s, and Q_h were calculated using average incoming solar radiation, combined with remotely sensed estimates of L_{ai} and surface albedo.

Global data fields of vapor pressure and temperature [time series (TS) 3.0] at 0.5° resolution came from the Climate Research Unit (New et al. 2000). Leaf area index and land cover type data at ~8-km resolution were obtained from Boston University (Ganguly et al. 2008a,b). Two precipitation datasets were examined—one from the Global Precipitation Climatology Project (GPCP, version 2; Adler et al. 2003) at 2.5° resolution, the other from the Global Precipitation Climatology Centre (GPCC, version 4; Rudolf and Schneider 2004) at 0.5° resolution. There was little difference between the two datasets at a common resolution of 2.5° (not shown), so the 0.5° GPCC dataset was used in the subsequent analyses.

Three global radiation products were used to calculate $\overline{E}_{Fu}$ and E_{PML}: 1) net short- and longwave radiation from the International Satellite Cloud Climatology Project (ISCCP) dataset (2.5° resolution; Zhang et al. 2004), 2) the Global Energy and Water Cycle Experiment Surface Radiation Budget products (SRB) at a 1.0° resolution (Gupta et al. 2006), and 3) the National Centers for Environmental Prediction (NCEP) and the National Center for Atmospheric Research (NCAR) reanalysis data (referred to as NCEP data) (Kalnay et al. 1996). All datasets were resampled to 0.5° spatial resolution. There are considerable differences in the annual global means and trends in available energy derived from the three datasets and we examine later

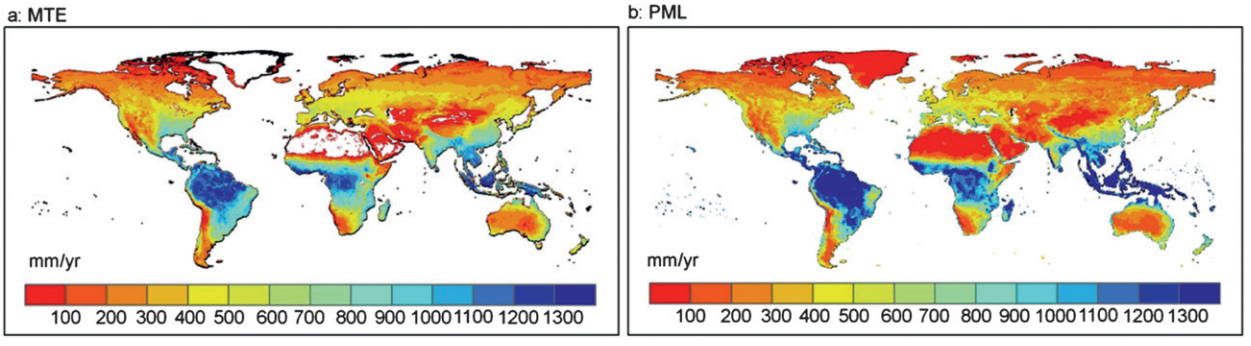

FIG. 3. Spatial patterns in (a) $\overline{E}_{MTE}$ and (b) $\overline{E}_{PML}$ averaged over 1983–2006 across global land surface.

TABLE 2. Correlation coefficient matrix between trends (1983–2006) in $\overline{E}_{MTE}$, $\overline{E}_{Fu}$, and $\overline{E}_{PML}$ for wet pixels where the aridity index $A_I \leq 1.5$ and for dry pixels where $A_I > 1.5$.

Pixels	Variables	Variables		
		$\overline{E}_{MTE}$	$\overline{E}_{PML}$	$\overline{E}_{Fu}$
Wet	$\overline{E}_{MTE}$	1.00	0.20	−0.02
	$\overline{E}_{PML}$		1.00	0.32
	$\overline{E}_{Fu}$			1.00
Dry	$\overline{E}_{MTE}$	1.00	0.53	0.49
	$\overline{E}_{PML}$		1.00	0.62
	$\overline{E}_{Fu}$			1.00

the consequences of these differences for E_{Fu} and E_{PML} (in Fig. 7 and Table 3).

Catchment water balances were calculated for 197 unregulated catchments over the hydrological year, defined as October–September to minimize effects of snowfall on yearly water balances (Dai et al. 2009). Selected catchments have an area >500 km^2 and missing daily streamflow data are less than 5% of the total. Streamflow data were from several sources: 1) 55 monthly series from the 925 gauges of Dai et al. (2009), 2) 53 daily series from the Global Runoff Data Centre streamflow database (http://www.bafg.de/GRDC/EN/Home/homepage__node.html), and 3) 88 daily series from Australia. Catchment boundaries were respectively delineated by 1) the Simulated Topological Network (STP-30p; Vorosmarty et al. 2000), 2) the HYDRO1k digital elevation model (DEM; Peel et al. 2010), and 3) the Australian GEODATA 9-s digital elevation model (Hutchinson 2002). Regulated catchments were identified from the 1) International Commission of Large Dams (Vorosmarty et al. 2003), 2) Meridian World Data (http://www.meridianworlddata.com/), and 3) National Land and Water Resources Audit of Australia (http://www.nlwra.gov.au/). It is noted that even in unregulated catchments, there may be changes in streamflow because the land is experiencing change draws of water for irrigation, flood control engineering, land use change, wetlands loss, etc. Such changes do not affect our analysis provided precipitation, evaporation, and runoff occur within the same catchment.

Trends in $\overline{E}_{wb}$, $\overline{E}_{Fu}$, E_{MTE} (or $\overline{E}_{MTE}$), E_{PML} (or $\overline{E}_{PML}$), and their inputs were calculated using the Mann–Kendall tau-b nonparametric technique including Sen's slope method (Sen 1968). This trend test is widely used in hydrology (Burn and Hag Elnur 2002). To minimize the effect of changes in interannual water storage on $\overline{E}_{wb}$, the trend test was applied to 5-yr moving averages for P and Q (Teuling et al. 2009). We recognize that a moving average increases the serial correlation (autocorrelation) of a data series. A prewhitening procedure, developed by Yue et al. (2002), was applied to each moving average series to eliminate the effect of serial correlation prior to applying the Mann–Kendall trend test in order to satisfy the test assumption of data independence. In addition, the data were also analyzed using 3-yr block averages (there are eight points for 23-yr time series) to check the consistency of the conclusions from the trends obtained using the 5-yr moving averages.

4. Results

Before examining trends in evaporation rates predicted by the methods described above, we first compare mean annual evaporation for 1983–2006 for the global land surface for "wet" pixels, where the aridity index $A_I = \overline{E}_p/\overline{P} \leq 1.5$, and "dry" pixels, where $A_I > 1.5$ (Table 1 and Fig. 1). Average global land surface evaporation estimated using the MTE approach of Jung et al. (2010) is $\overline{E}_{MTE}$ = 521.5 mm yr^{-1}, while Mueller et al. (2011) reported a value of 45.3 ± 5.7 W m^{-2} (572.4 ± 68.4 mm yr^{-1}) from an analysis of 40 global evaporation datasets. Using the ISCCP radiation data, we estimated $\overline{E}_{PML}$ = 563.2 mm yr^{-1}, which is a difference of ±4% relative to the mean of the two, and $\overline{E}_{MTE}$ and $\overline{E}_{PML}$ differ by ±6% for wet pixels and only ±2% for dry pixels. The two approaches give similar values for the annual average volume of water evaporated globally, and both are in excellent agreement with estimates given by Oki and Kanae (2006). The average of these three estimates is 11% less than that of Trenberth et al. (2007).

Time series of anomalies in annual E_{MTE} and E_{PML} relative to their respective means are shown in Fig. 2 for the global land surface and for wet and dry pixels. We see that interannual variation in E_{PML} is greater than for E_{MTE} in all three panels and that the variation in E_{PML} is greatest for wet pixels. There is a statistically significant increasing trend in the evaporation anomalies for all three classes ($p < 0.01$), but the slope of 1.088 mm yr^{-1} in the global trend for annual E_{PML} is almost double that of 0.528 mm yr^{-1} for E_{MTE}. Trends predicted using annual E_{PML} are also double those from E_{MTE} for wet and dry catchments.

Patterns of 23-yr average evaporation rates $\overline{E}_{MTE}$ across the global land surface are very similar to those for $\overline{E}_{PML}$ (Fig. 3), with both models giving high rates in tropical and wet regions such as in the Amazon and Congo basins and low evaporation rates in arid and high-latitude regions, such as in central Australia and Siberia. We note that $\overline{E}_{MTE}$ is not available for the Sahara Desert and Greenland. There is a high degree of spatial correlation between $\overline{E}_{MTE}$ and $\overline{E}_{PML}$: r = 0.90 for wet pixels and r = 0.81 for dry pixels. Note that the average patterns

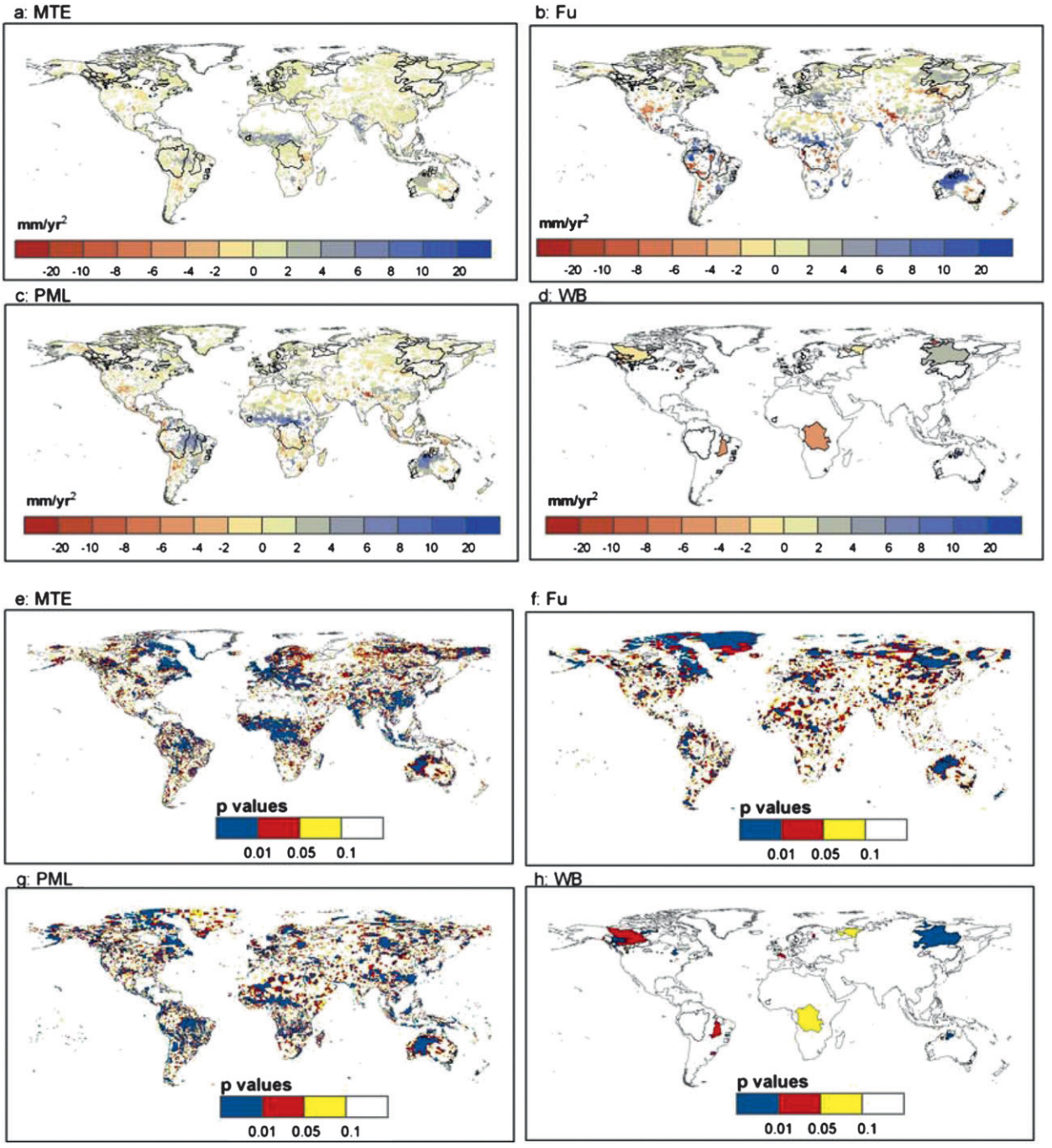

FIG. 4. Global map of trends in (a) $\overline{E}_{\mathrm{MTE}}$, (b) $\overline{E}_{\mathrm{Fu}}$, (c) $\overline{E}_{\mathrm{PML}}$, and (d) $\overline{E}_{\mathrm{wb}}$ from 1983 to 2006. (e)–(h) The corresponding two-sided p values for each grid cell obtained from the prewhitened Mann–Kendall trend test. Grid cells in all panels are left blank when $p > 0.1$. Boundaries for the 197 unregulated catchments are shown in black.

of $\overline{E}_{\mathrm{Fu}}$ and $\overline{E}_{\mathrm{PML}}$ are identical for reasons explained in section 2c.

While there is good agreement between the global patterns in $\overline{E}_{\mathrm{MTE}}$ and $\overline{E}_{\mathrm{PML}}$ averaged over the 23-yr study period, this is not the case for the trends in evaporation from wet catchments as calculated using the two approaches (Table 2). There is essentially no correlation between trends in $\overline{E}_{\mathrm{MTE}}$ and those in $\overline{E}_{\mathrm{Fu}}$ and a correlation coefficient of only 0.32 for $\overline{E}_{\mathrm{PML}}$ versus $\overline{E}_{\mathrm{Fu}}$ (Table 2). A better relationship amongst the three is found for dry

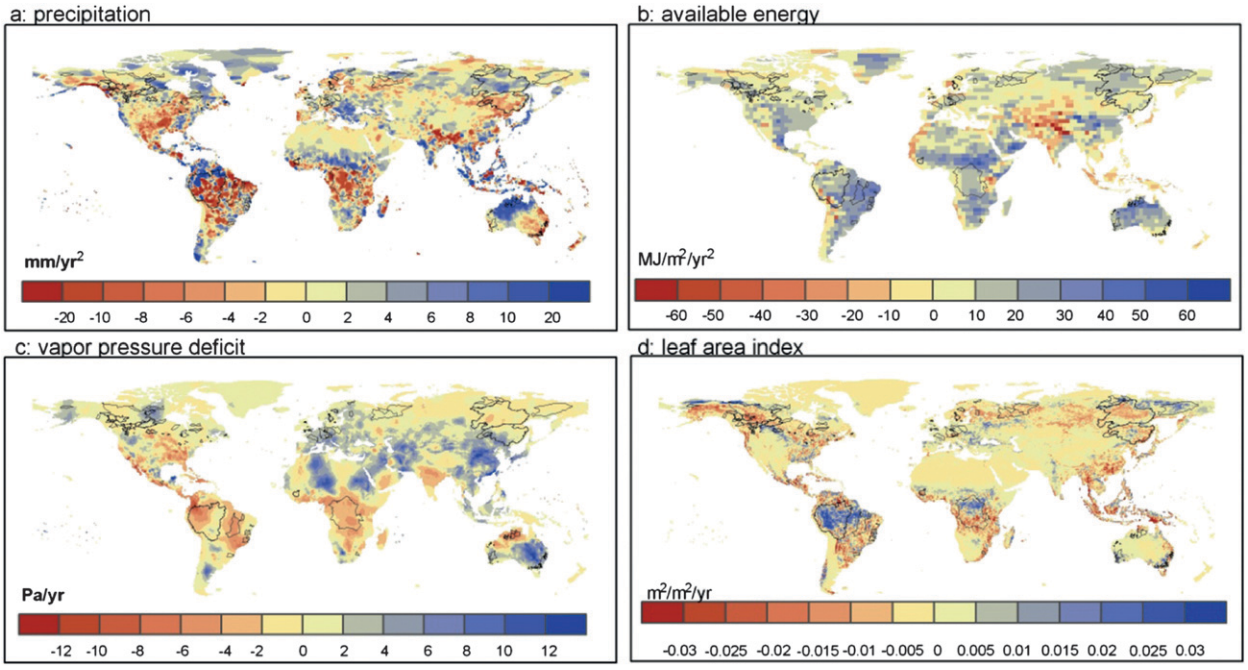

FIG. 5. Global map of trends (1983–2006) in (a) precipitation, $\overline{P}$; (b) available energy, A; (c) vapor pressure deficit, D; and (d) leaf area index, L_{ai}. Boundaries for the 197 unregulated catchments are shown in black.

catchments, where the correlation coefficient is ~0.5 for $\overline{E}_{MTE}$ versus $\overline{E}_{Fu}$ or $\overline{E}_{PML}$, and ~0.6 for $\overline{E}_{Fu}$ versus $\overline{E}_{PML}$.

Figures 4a–d show global maps of average trends in $\overline{E}_{MTE}$, $\overline{E}_{Fu}$, and $\overline{E}_{PML}$ for each 0.5° land surface pixel and Figs. 4e–h show maps of the corresponding probability (p) values for statistical significance. Estimated trends in $\overline{E}_{MTE}$ are a positive 2–6 mm yr^{-1} across equatorial Africa, India, and northwest Australia with $p < 0.05$, but they are quite small across the rest of the globe. In contrast, $\overline{E}_{Fu}$ and $\overline{E}_{PML}$ show increasing and decreasing trends across different regions. Both suggest significant ($p = 0.05$) decreasing trends in the southwestern United States, the Himalayas, and parts of Africa and South America, with increasing trends for equatorial Africa, northwest Australia, and the northeastern United States. It is very difficult to validate these trend estimates using $\overline{E}_{wb}$ because of the small number of unregulated catchments that still remain across the globe. Trends indicated by $\overline{E}_{Fu}$ and $\overline{E}_{PML}$ in northern Australia, northwestern Canada, and eastern Siberia are similar to trends in $\overline{E}_{wb}$ for those regions, but catchment water balances indicate negative trends in $\overline{E}_{wb}$ for subequatorial Africa and northeastern Brazil, opposite to those in $\overline{E}_{Fu}$ and $\overline{E}_{PML}$. The trend in $\overline{E}_{wb}$ is not significant ($p > 0.1$) in the Amazon basin, whereas $\overline{E}_{Fu}$ shows a mixture of positive and negative trends and $\overline{E}_{PML}$ suggests positive trends (Fig. 4).

Global maps of trends in the key drivers of evaporation—precipitation $\overline{P}$, available energy A, humidity deficit D, and leaf area index L_{ai}—are shown in Fig. 5. Most striking is the strong positive trend in remotely sensed available energy (ISCCP forcing) in the central United States and in much of the Southern Hemisphere, especially in Brazil and central Africa. These are generally accompanied by strong negative trends in $\overline{P}$, small decreasing trends in D, and increasing L_{ai}, whereas the positive trend in A for the northwest of Australia is associated with an increase in $\overline{P}$ and a decrease in D. Sensitivity analyses showed that trends in D and L_{ai} observed in Fig. 5 do not explain the trends in $\overline{E}_{PML}$ seen in Fig. 4 (data not shown). Instead, precipitation mainly controls evaporation in dry catchments ($A_I > 1.5$), whereas evaporation from wet catchments ($A_I \leq 1.5$) is largely determined by available energy. This is consistent with (Fisher et al. 2009), who found that A accounts for 87% of the variance in E measured at 31 flux stations in Amazonia.

Values of $\overline{E}_{Fu}$ and E_{PML} (or $\overline{E}_{PML}$) presented thus far were calculated using ISCCP radiation data, but the SRB and NCEP global radiation datasets were also available for analysis (section 3). We note that radiation data are not used to calculate E_{MTE}, which is estimated using evaporation measurements from the global FLUXNET database, gridded global meteorological data, and remotely sensed fraction of absorbed photosynthetically active radiation (Jung et al. 2010). In Fig. 6 we compare maps of trends in available energy constructed using the three datasets and in Fig. 7 we examine the

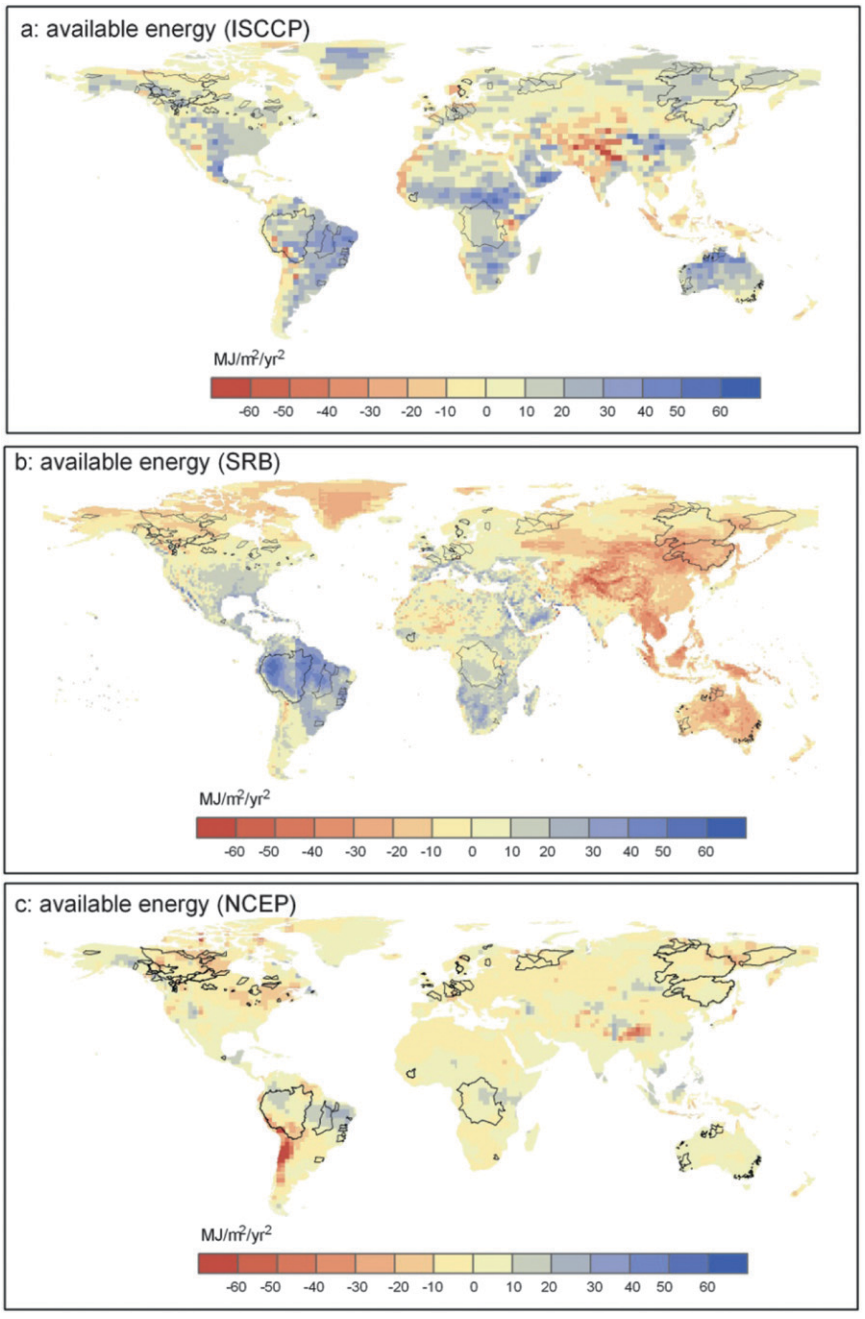

FIG. 6. Trends (1983–2006) in available energy from (a) the ISCCP radiation products (Zhang et al. 2004), (b) the SRB (Gupta et al. 2006), and (c) the NCEP–NCAR reanalysis data (Kalnay et al. 1996). Boundaries for the 197 unregulated catchments are shown in black.

effects of alternative estimates of available energy on the calculated trends in annual E_{PML} (note that $\overline{E}_{\mathrm{Fu}}$ is only available at a mean annual scale). Figure 6 shows that there are clear differences in the magnitudes, sign, and patterns between the three datasets, with ISCCP and SRB showing positive trends in A over South America and Africa that are not apparent in the NCEP dataset. The SRB dataset shows strong negative trends in A over Asia but such trends are not seen in the other two radiation products. These differences can be seen more quantitatively when the radiation data are applied to the 110 wet catchments used in this study. Substantial differences in mean trends in annual available energy are calculated using the ISCCP, SRB, and NCEP

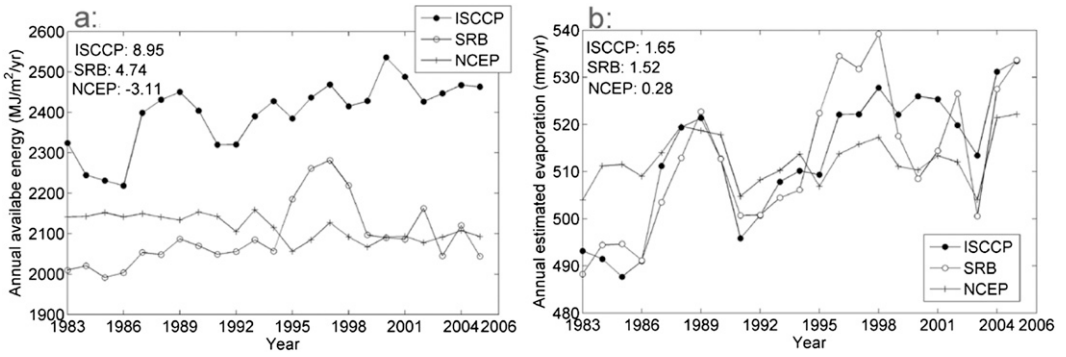

FIG. 7. Time series of annual A and E_{PML}, both aggregated from grids of the 110 wet catchments. Values after colons are the mean trend slopes. The offset in A between the ISCCP and SRB datasets does not appear in trends in E_{PML} because E_{PML} is constrained by the Fu (1981) hydrometeorological model using each radiation dataset independently.

data: 8.95, 4.74, and −3.11 MJ m^{-2} yr^{-2}, respectively (Fig. 7a). When these radiation datasets are used with the PML model, the corresponding mean trends in annual E_{PML} are 1.65, 1.52, and 0.28 mm yr^{-1} (Fig. 7b). Note that the offset in A between the ISCCP and SRB datasets does not appear in the trends in E_{PML} because annual E_{PML} is constrained by the Fu (1981) hydrometeorological model using each radiation dataset independently (section 2). The negative trend in A seen in the NCEP dataset is not apparent in the trend in E_{PML} because of compensating trends in the other variables affecting E_{PML}.

The results presented in Figs. 1–7 are for pixels across the global land surface. In Figs. 8 and 9, trend analysis is conducted for 110 unregulated wet and 87 dry catchments for which we calculated $\overline{E}_{wb}$. Figure 8 shows there is no correlation between trends in $\overline{E}_{wb}$ and $\overline{E}_{MTE}$ and weak but significant correlation between $\overline{E}_{wb}$ and $\overline{E}_{PML}$ or $\overline{E}_{Fu}$ at $p = 0.1$ for wet catchments. Correlations between $\overline{E}_{wb}$ and $\overline{E}_{MTE}$, $\overline{E}_{PML}$, and $\overline{E}_{wb}$ are all significant at $p = 0.001$ for dry catchments but the regression slope for the MTE method and the PML model are much less than unity. Only the Fu model results in a desired linear regression slope close to one and a high R^2 value. This is because precipitation appears explicitly in the Fu model [Eq. (2)] and because in dry catchments trends in $\overline{E}_{wb}$ are highly correlated to those in P (Fig. 9b). The inclusion of P in the Fu model clearly improves predictions of trends in E for dry catchments where $\overline{P} \approx \overline{E}$, but not for wet catchments where there is only a weak correlation between trends in $\overline{P}$ and $\overline{E}_{wb}$ (Fig. 9a).

Trends in $\overline{E}_{PML}$ and $\overline{E}_{Fu}$ for the 197 catchments were also calculated using the SRB and NCEP available energy data. Table 3 shows statistics comparing trends in $\overline{E}_{PML}$ and $\overline{E}_{Fu}$ with those in $\overline{E}_{wb}$. Although the ISCCP product has the coarsest spatial resolution (2.5°) amongst the three, the trends in $\overline{E}_{Fu}$ and $\overline{E}_{PML}$ estimated by the ISCCP product have the best linear correlation to those in $\overline{E}_{wb}$ (Table 3). This is highlighted in wet catchments where both trends in $\overline{E}_{PML}$ and $\overline{E}_{Fu}$ forced by the ISCCP data are significantly correlated ($p = 0.053$) to those in $\overline{E}_{wb}$, but not for the trends obtained from the other two. In dry catchments, trends in $\overline{E}_{PML}$ forced by the ISCCP data have the highest R^2 values while those for trends in $\overline{E}_{Fu}$ forced by the three radiation products are almost the same.

The results shown in Figs. 8 and 9 may be biased because they were obtained from 5-yr moving averages, which can increase the serial correlation in the data. However, recalculation of the trends in $\overline{E}_{MTE}$, $\overline{E}_{PML}$, $\overline{E}_{Fu}$, and $\overline{E}_{wb}$ using 3-yr block averages yielded similar results (data not shown); that is, weak but significant correlation between $\overline{E}_{wb}$ and $\overline{E}_{PML}$ and $\overline{E}_{Fu}$ but not between $\overline{E}_{wb}$ and $\overline{E}_{MTE}$ in wet catchments, and strong correlation in dry catchments.

The values of $\overline{E}_{wb}$ used above rely on data from a range of catchment sizes. Small-area catchments typically cover one to several of the 0.5° pixels of the GPCC precipitation data, and combining these with local runoff measurements could inflate trends in $\overline{E}_{wb}$ (i.e., $\overline{P} - \overline{Q}$) compared to larger catchments. To examine whether this adversely affects the results shown in Fig. 8, we identified 107 small-area catchments (500–5000 km^2) and 90 large-area catchments (>5000 km^2). Results from the two groups (not shown) are similar to those shown in Fig. 8—that is, trends in $\overline{E}_{wb}$ compare well to those in $\overline{E}_{MTE}$, $\overline{E}_{PML}$, and $\overline{E}_{Fu}$ in dry catchments, but not in wet catchments. Yang et al. (2007) also found that catchment area did not change the relationship between $\overline{E}_{wb}$ and $\overline{E}_{Fu}$ for 108 catchments in China with areas varying from 200 to 100 000 km^2.

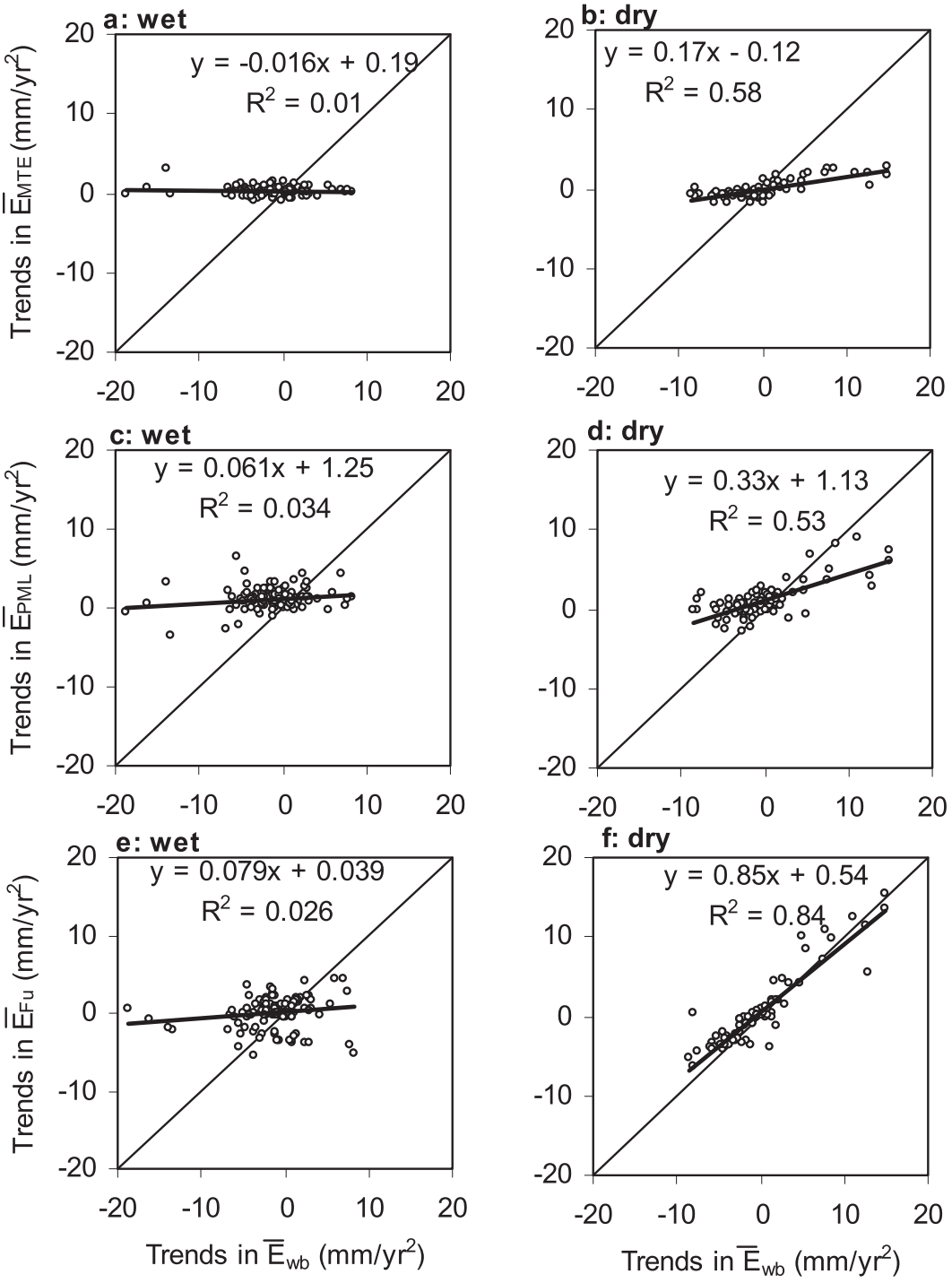

FIG. 8. Comparison of trends in $\overline{E}_{\mathrm{MTE}}$, $\overline{E}_{\mathrm{PML}}$, and $\overline{E}_{\mathrm{Fu}}$ estimated using the ISCCP radiation data vs $\overline{E}_{\mathrm{wb}}$ for (a),(c),(e) 110 wet catchments and (b),(d),(f) 87 dry catchments.

5. Discussion

Our analysis has shown that decadal trends in evaporation calculated using water balances, $\overline{E}_{\mathrm{wb}}$ of 110 wet catchments are not matched by trends in $\overline{E}_{\mathrm{MTE}}$. This model-tree ensemble approach of Jung et al. (2010) uses statistical relationships between evaporation rates measured at 253 globally distributed flux stations and meteorological

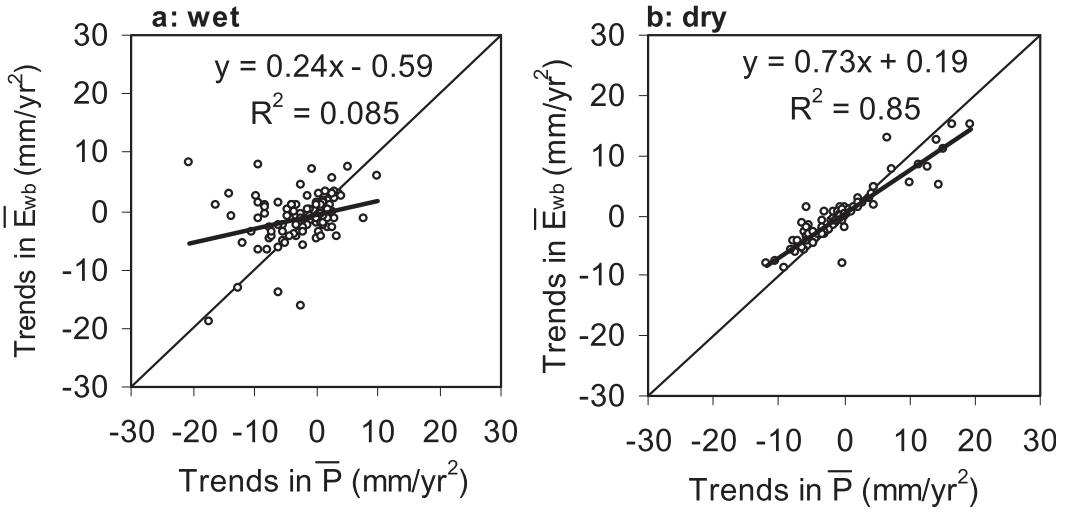

FIG. 9. Comparison of trends in $\overline{E}_{wb}$ and $\overline{P}$ for (a) 110 wet catchments and (b) 87 dry catchments.

drivers, including remotely sensed fraction of photosynthetically active radiation. Similarly in wet catchments there are only weak correlation between trends in $\overline{E}_{wb}$ and $\overline{E}_{Fu}$, a hydrometeorological model, and between $\overline{E}_{wb}$ and $\overline{E}_{PML}$, which is calculated using the Penman–Monteith energy-balance equation coupled with a simple biophysical model for surface conductance. The lack of correlation between $\overline{E}_{wb}$ and any of $\overline{E}_{MTE}$, $\overline{E}_{Fu}$, or $\overline{E}_{PML}$ may be due to uncertainties in $\overline{E}_{wb}$ caused by errors in runoff and precipitation data for the selected catchments. Catchment runoff data are measured directly and hence are considered the most reliable in this study. Errors in precipitation can be quite large in regions where spatial interpolation is based on a sparse network of rain gauges (Oki et al. 1999). Such uncertainties are unlikely to explain the lack of correlation because identical conclusions are reached using two global precipitation datasets [GPCC: 0.5° grid cells (Rudolf and Schneider 2004) or GPCP: 2.5° resolution (Adler et al. 2003)]. A mismatch in scale between runoff and precipitation data may contribute to large trend values in $\overline{E}_{wb}$ ($>\pm 10$ mm yr^{-1}) in relatively small catchments ($<50\,000$ km^2).

We note that remotely sensed radiation is a key input to the two structurally different diagnostic models (E_{PML} and E_{Fu}) and thus the lack of correlation between trends in these quantities and $\overline{E}_{wb}$ for wet catchments seen in Fig. 8 may result from uncertainties in magnitudes and trends in available energy. Evidence for this is seen in Fig. 6 where trends in A calculated using two remotely sensed radiation (ISCCP and SRB) datasets and one global forecast model data product (NCEP) result in quite different patterns globally and for the catchments analyzed in this paper (Fig. 7). These results suggest that radiation data derived from satellites may not yet be sufficiently accurate to explain trends in evaporation at global and regional scales over the past quarter century.

Model structural limitations as well as errors in input data may be responsible for the discrepancies in trends in $\overline{E}_{wb}$ compared to those in $\overline{E}_{MTE}$, $\overline{E}_{Fu}$, or $\overline{E}_{PML}$. In a multimodel comparison study, Mueller et al. (2011) found that simple diagnostic models as used in this study provided means and standard deviations of E in global datasets that were similar to estimates from more complex land surface models and reanalysis datasets. All models yielded uncertainties that exceeded 20% of mean

TABLE 3. Regressions for trends in $\overline{E}_{PML}$ and $\overline{E}_{Fu}$ vs those in $\overline{E}_{wb}$ for wet and dry catchments, respectively. Here $y = \overline{E}_{PML}$ or $\overline{E}_{Fu}$, and $x = \overline{E}_{wb}$ (mm yr^{-2}).

Models	Available energy products	Wet catchments	R^2	p values	Dry catchments	R^2	p values
PML	ISCCP	$y = 0.061x + 1.25$	0.034	0.053	$y = 0.33x + 1.13$	0.53	0.00
	SRB	$y = -0.02x + 0.46$	0.02	0.68	$y = 0.33x - 0.77$	0.44	0.00
	NCEP	$y = 0.012x + 0.36$	0.0016	0.68	$y = 0.25x + 0.54$	0.39	0.00
Fu	ISCCP	$y = 0.079x + 0.039$	0.026	0.093	$y = 0.85x + 0.54$	0.84	0.00
	SRB	$y = -0.023x - 0.54$	0.001	0.73	$y = 0.85x - 0.33$	0.86	0.00
	NCEP	$y = -0.0073x - 0.70$	0.0003	0.85	$y = 0.82x + 0.32$	0.86	0.00

evaporation fluxes in most regions of the globe, and Mueller et al. (2011) concluded that further collections of ''ground truth'' observations are needed to constrain model estimates of evaporation. Given such uncertainties in the fluxes themselves, it is perhaps not surprising that we are unable to reconcile trends in land surface evaporation from water balance studies with those from models using the currently available forcing data.

6. Conclusions

Improvements are needed in global datasets of precipitation, runoff, radiation, and meteorological forcing before we can be confident in model estimates of the magnitude and sign of trends in evaporation from land surfaces. Effective combination of precipitation and soil moisture information with satellite radiation and vegetation data will undoubtedly improve estimation of trends in global E by hydrological models in the future.

Acknowledgments. Aiguo Dai provided monthly streamflow data for the 925 global river basins, and the Global Runoff Data Centre, Koblen, Germany provided daily streamflow data for 107 gauges. We thank Dr. Chris Smith, Dr. Michael Roderick, and two anonymous reviewers for their helpful comments.

REFERENCES

Adler, R. F., and Coauthors, 2003: The Version-2 Global Precipitation Climatology Project (GPCP) Monthly Precipitation Analysis (1979–present). *J. Hydrometeor.,* **4,** 1147–1167.

Burn, D. H., and M. A. Hag Elnur, 2002: Detection of hydrologic trends and variability. *J. Hydrol.,* **255,** 107–122.

Dai, A., T. T. Qian, K. E. Trenberth, and J. D. Milliman, 2009: Changes in continental freshwater discharge from 1948 to 2004. *J. Climate,* **22,** 2773–2792.

Fisher, J. B., and Coauthors, 2009: The land–atmosphere water flux in the tropics. *Global Change Biol.,* **15,** 2694–2714.

Fu, B. P., 1981: On the calculation of the evaporation from land surface (in Chinese). *Sci. Atmos. Sin.,* **5,** 23–31.

Ganguly, S., M. A. Schull, A. Samanta, N. V. Shabanov, C. Milesi, R. R. Nemani, Y. Knyazikhin, and R. B. Myneni, 2008a: Generating vegetation leaf area index earth system data record from multiple sensors. Part 1: Theory. *Remote Sens. Environ.,* **112,** 4333–4343.

——, A. Samanta, M. A. Schull, N. V. Shabanov, C. Milesi, R. R. Nemani, Y. Knyazikhin, and R. B. Myneni, 2008b: Generating vegetation leaf area index earth system data record from multiple sensors. Part 2: Implementation, analysis and validation. *Remote Sens. Environ.,* **112,** 4318–4332.

Gedney, N., P. M. Cox, R. A. Betts, O. Boucher, C. Huntingford, and P. A. Stott, 2006: Detection of a direct carbon dioxide effect in continental river runoff records. *Nature,* **439,** 835–838.

Gupta, S. K., P. W. Stackhouse, S. J. Cox, J. C. Mikovitz, and T. P. Zhang, 2006: 22-year surface radiation budget data set. *GEWEX News,* Vol. 16, No. 4, International GEWEX Project Office, Silver Spring, MD, 12–13.

Huntington, T. G., 2006: Evidence for intensification of the global water cycle: Review and synthesis. *J. Hydrol.,* **319,** 83–95.

Hutchinson, M. F., Ed., 2002: GEODATA 9 Second DEM (version 2.1): Data user guide. GeoScience Australia, 43 pp.

Isaac, P. R., R. Leuning, J. M. Hacker, H. A. Cleugh, P. A. Coppin, O. T. Denmead, and M. R. Raupach, 2004: Estimation of regional evapotranspiration by combining aircraft and ground-based measurements. *Bound.-Layer Meteor.,* **110,** 69–98.

Jung, M., M. Reichstein, and A. Bondeau, 2009: Towards global empirical upscaling of FLUXNET eddy covariance observations: Validation of a model tree ensemble approach using a biosphere model. *Biogeosciences,* **6,** 2001–2013.

——, and Coauthors, 2010: Recent decline in the global land evapotranspiration trend due to limited moisture supply. *Nature,* **467,** 951–954.

Kalnay, E., and Coauthors, 1996: The NCEP/NCAR 40-Year Reanalysis Project. *Bull. Amer. Meteor. Soc.,* **77,** 437–471.

Le Moine, N., V. Andréassian, C. Perrin, and C. Michel, 2007: How can rainfall-runoff models handle intercatchment groundwater flows? Theoretical study based on 1040 French catchments. *Water Resour. Res.,* **43,** W06428, doi:10.1029/2006WR005608.

Leuning, R., Y. Q. Zhang, A. Rajaud, H. Cleugh, and K. Tu, 2008: A simple surface conductance model to estimate regional evaporation using MODIS leaf area index and the Penman-Monteith equation. *Water Resour. Res.,* **44,** W10419, doi:10.1029/2007WR006562.

Milly, P. C. D., K. A. Dunne, and A. V. Vecchia, 2005: Global pattern of trends in streamflow and water availability in a changing climate. *Nature,* **438,** 347–350.

Monteith, J. L., 1964: Evaporation and environment: The state and movement of water in living organisms. *19th Symp. of the Society of Experimental Biology,* Cambridge University Press, 205–234.

Mueller, B., and Coauthors, 2011: Evaluation of global observations-based evapotranspiration datasets and IPCC AR4 simulations. *Geophys. Res. Lett.,* **38,** L06402, doi:10.1029/2010gl046230.

New, M., M. Hulme, and P. Jones, 2000: Representing twentieth-century space–time climate variability. Part II: Development of 1901–96 monthly grids of terrestrial surface climate. *J. Climate,* **13,** 2217–2238.

Oki, T., and S. Kanae, 2006: Global hydrological cycles and world water resources. *Science,* **313,** 1068–1072.

——, T. Nishimura, and P. Dirmeyer, 1999: Assessment of annual runoff from land surface models using Total Runoff Integrating Pathways (TRIP). *J. Meteor. Soc. Japan,* **77,** 235–255.

Peel, M. C., T. A. McMahon, and B. L. Finlayson, 2010: Vegetation impact on mean annual evapotranspiration at a global catchment scale. *Water Resour. Res.,* **46,** W09508, doi:10.1029/2009WR008233.

Piao, S. L., P. Friedlingstein, P. Ciais, N. de Noblet-Ducoudre, D. Labat, and S. Zaehle, 2007: Changes in climate and land use have a larger direct impact than rising CO_2 on global river runoff trends. *Proc. Natl. Acad. Sci. USA,* **104,** 15 242–15 247.

Priestley, C. H. B., and R. J. Taylor, 1972: On the assessment of surface heat flux and evaporation using large-scale parameters. *Mon. Wea. Rev.,* **100,** 81–92.

Roderick, M. L., and G. D. Farquhar, 2002: The cause of decreased pan evaporation over the past 50 years. *Science,* **298,** 1410–1411.

Rudolf, B., and U. Schneider, 2004: Calculation of gridded precipitation data for the global land-surface using in-situ gauge observations. *Proc. Second Workshop of the Int. Precipitation Working Group,* Monterey, CA, IPWG, 231–247.

Sen, P. K., 1968: Estimates of regression coefficient based on Kendall's tau. *J. Amer. Stat. Assoc.,* **63,** 1379–1389.

Teuling, A. J., and Coauthors, 2009: A regional perspective on trends in continental evaporation. *Geophys. Res. Lett.,* **36,** L02404, doi:10.1029/2008GL036584.

Trenberth, K. E., L. Smith, T. T. Qian, A. Dai, and J. Fasullo, 2007: Estimates of the global water budget and its annual cycle using observational and model data. *J. Hydrometeor.,* **8,** 758–769.

Vorosmarty, C. J., B. M. Fekete, M. Meybeck, and R. B. Lammers, 2000: Global system of rivers: Its role in organizing continental land mass and defining land-to-ocean linkages. *Global Biogeochem. Cycles,* **14,** 599–621.

——, M. Meybeck, B. Fekete, K. Sharma, P. Green, and J. P. M. Syvitski, 2003: Anthropogenic sediment retention: Major global impact from registered river impoundments. *Global Planet. Change,* **39,** 169–190.

Wild, M., and Coauthors, 2005: From dimming to brightening: Decadal changes in solar radiation at Earth's surface. *Science,* **308,** 847–850.

——, J. Grieser, and C. Schaer, 2008: Combined surface solar brightening and increasing greenhouse effect support recent intensification of the global land-based hydrological cycle. *Geophys. Res. Lett.,* **35,** L17706, doi:10.1029/2008GL034842.

Yang, D. W., F. B. Sun, Z. Y. Liu, Z. T. Cong, G. H. Ni, and Z. D. Lei, 2007: Analyzing spatial and temporal variability of annual water-energy balance in nonhumid regions of China using the Budyko hypothesis. *Water Resour. Res.,* **43,** W04426, doi:10.1029/2006WR005224.

Yue, S., P. Pilon, B. Phinney, and G. Cavadias, 2002: The influence of autocorrelation on the ability to detect trend in hydrological series. *Hydrol. Processes,* **16,** 1807–1829.

Zhang, L., W. R. Dawes, and G. R. Walker, 2001: Response of mean annual evapotranspiration to vegetation changes at catchment scale. *Water Resour. Res.,* **37,** 701–708.

Zhang, X. B., F. W. Zwiers, G. C. Hegerl, F. H. Lambert, N. P. Gillett, S. Solomon, P. A. Stott, and T. Nozawa, 2007: Detection of human influence on twentieth-century precipitation trends. *Nature,* **448,** 461–465.

Zhang, Y. C., W. B. Rossow, A. A. Lacis, V. Oinas, and M. I. Mishchenko, 2004: Calculation of radiative fluxes from the surface to top of atmosphere based on ISCCP and other global data sets: Refinements of the radiative transfer model and the input data. *J. Geophys. Res.,* **109,** D19105, doi:10.1029/2003JD004457.

Zhang, Y. Q., R. Leuning, L. B. Hutley, J. Beringer, I. McHugh, and J. P. Walker, 2010: Using long-term water balances to parameterize surface conductances and calculate evaporation at 0.05° spatial resolution. *Water Resour. Res.,* **46,** W05512, doi:10.1029/2009WR008716.